

Journal Pre-proof

Effect of pre-activation treatment temperature on hydrodesulfurization catalytic activity of CoMoS/KIT-6

Karen A. Beltrán, Lorena Alvarez-Contreras, Anabel D. Delgado, César C. Leyva-Porras, Alfredo Aguilar-Elguezabal



PII: S0920-5861(19)30553-X
DOI: <https://doi.org/10.1016/j.cattod.2019.10.019>
Reference: CATTOD 12524

To appear in: *Catalysis Today*

Received Date: 16 February 2019
Revised Date: 28 September 2019
Accepted Date: 1 October 2019

Please cite this article as: Beltrán KA, Alvarez-Contreras L, Delgado AD, Leyva-Porras CC, Aguilar-Elguezabal A, Effect of pre-activation treatment temperature on hydrodesulfurization catalytic activity of CoMoS/KIT-6, *Catalysis Today* (2019), doi: <https://doi.org/10.1016/j.cattod.2019.10.019>

This is a PDF file of an article that has undergone enhancements after acceptance, such as the addition of a cover page and metadata, and formatting for readability, but it is not yet the definitive version of record. This version will undergo additional copyediting, typesetting and review before it is published in its final form, but we are providing this version to give early visibility of the article. Please note that, during the production process, errors may be discovered which could affect the content, and all legal disclaimers that apply to the journal pertain.

© 2019 Published by Elsevier.

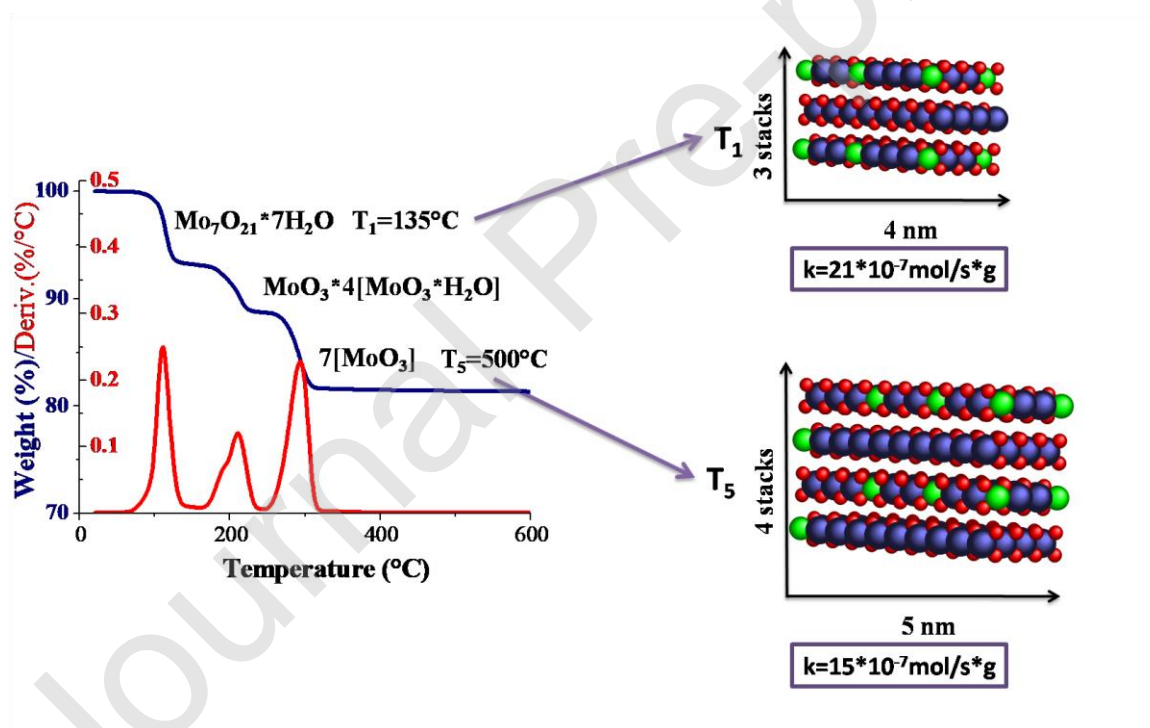
Effect of pre-activation treatment temperature on hydrodesulfurization catalytic activity of CoMoS/KIT-6

Karen A. Beltrán, Lorena Alvarez-Contreras*, Anabel D. Delgado, César C. Leyva-Porras, Alfredo Aguilar-Elguezabal.

Centro de Investigación en Materiales Avanzados, S. C. Miguel de Cervantes No. 120, Complejo Industrial Chihuahua, Chih., México, CP 31136.

*Corresponding author: lorena.alvarez@cimav.edu.mx

Graphical abstract



Highlights.

- CoMoS/KIT-6 catalysts with different pre-activation thermal treatments were synthesized.
- Metal loading of 16% wt. CoMo was used.

- Lower pre-activation temperatures lead to smaller and less stacked CoMoS crystals.
- Pre-activation thermal treatment is a key factor to improve catalytic activity.

Abstract

Mesoporous silica-supported cobalt–molybdenum hydrodesulfurization catalysts have been prepared by wetness impregnation, drying and a thermal pre-treatment of impregnated support before activation. Characterization of materials was made by nitrogen adsorption, thermogravimetric analysis, Raman spectroscopy, TEM and XPS. Catalytic activity was determined by hydrodesulfurization of dibenzothiophene (DBT). The results indicate that the thermal pre-treatment carried out at the lower temperature allows the formation of smaller and less stacked active phase structures, with a higher amount of CoMoS phase.

Keywords

Ordered mesoporous silica, supported HDS catalysts, CoMoS catalysts, KIT-6

1. Introduction.

Due to the environmental damages associated to the release of sulfur compounds as a consequence of fuels burning and the increasing demand for fuels, environmental laws have become stricter in sulfur content in these substances, nowadays in many countries the maximum content of sulfur must be lower than 10 ppm[1–5]. This requirement on fuels promotes the adjustment of hydrotreatment processes on crude oil refineries, some of these improvements include the development of more active catalysts, i.e., with modifications of morphology or composition of supports, active phases or even the use of additives, among other changes[6–12]. For hydrodesulfurization (HDS) processes it is known that the key in obtaining a highly active catalyst is related to the crystalline structure, and the most accepted model is the formation of the so-called CoMoS phase[13,14], where electronic effects induced by the insertion of Co promoter facilitate the removal of the sulfur atom from molecules that contain this atom in its structure, moreover Ramos et al proposed that Co also modifies textural and structural properties of MoS₂ slabs [15]. Effect of activation treatments on metals sulfidation degree has been scarcely studied. Some of the important steps to modulate the formation of sulfides of active phases are the gas flow, H₂S/H₂ ratio, time of treatment and temperature, although another important characteristic is the chemical structure of precursors of active phase before activation step.

In order to obtain ultra-low sulfur content diesel, is essential to remove sulfur from refractory molecules such as dibenzothiophenes and alkyl dibenzothiophenes, like 4,6-dimethyldibenzothiophene, making this task a challenge [3,5,16–20]. Thus, to reach environmental regulations, researchers have focused on the development of more effective catalysts for deep removal of sulfur, considering also the reduction of processing costs by lowering the severity of the reaction conditions such as hydrogen pressure and temperature.

The material most used as support of HDS catalyst is gamma-alumina [21–24], nevertheless researchers have also explored other materials like nanostructured silica (SBA-15, MCM-41 and KIT-6) [2,4,25–32]. Particularly, KIT-6 is a mesoporous silica with tridimensional interconnected channels that makes this material a promising support for HDS catalysts. KIT-6 has high surface area and pore diameter over 6 nm, that allows better metal dispersion and the diffusion of large molecules through pores, moreover KIT-6 has thermal and mechanical stability [2,4]. This work demonstrates that there is an effect of thermal treatment of precursors once impregnated on support and previously to activation treatment, on the activity for hydrodesulfurization, which is due to the dispersion and structure of active phases obtained.

2. Materials and methods

Synthesis of catalyst consists on preparation of support, impregnation of cobalt precursor on support, after that impregnation of molybdenum precursor, then thermal treatment, and finally, the activation step. Catalysts were synthesized with 16% wt. total metal loading (11.2 % wt. of Mo and 4.8% wt. of Co).

2.1. Supports Impregnation

The synthesis of KIT-6 (mesoporous silica) was made according to the modified methodology previously reported by Freddy Kleitz et al. [33]. Triblock copolymer (pluronic P 123 from Sigma Aldrich) was used as structure-directing agent. Synthesis is as follows: for a typical synthesis, pluronic P123 (15.9 g) is dissolved in a mixture of distilled water (575 mL) and hydrochloric acid (26.3 mL, J. T. Baker 36.5-38 %), later, butanol (19.6 mL, Sigma Aldrich 99.8 %) is added under constant stirring at 308 K. After 1 h, tetraethyl orthosilicate (36.6 mL TEOS, Sigma Aldrich 98%) was added dropwise under continuous stirring for 2 h at 308 K. The solution was then transferred to a Teflon autoclave heated at 393 K for 24 h.

Finally, the solid was filtered, washed with a mixture of ethanol (HYCEL 96 %) and hydrochloric acid and dried, followed by calcination at 823 K to remove the template. Then wetness impregnation of precursor salts was made; firstly, an appropriate amount of cobalt nitrate 6-hydrate (from J. T. Baker 99.1% of purity) in aqueous solution was used for impregnation. Subsequently, the impregnated support was dried during 2h at 60 °C. In a second step, a solution of ammonium heptamolybdate tetrahydrate ((NH₄)₆Mo₇O₂₄, HMA, from Sigma Aldrich 99.9% of purity) was used as molybdenum precursor. The obtained sample were then calcined at 135, 225, 300, 450, or 500 °C for 3 h with a heating rate of 4 °C/min, and the CoMo catalysts precursors were named as is shown in the Table 1.

2.2. Catalysts Activation.

The activation of catalysts was made “ex-situ”. For this purpose, the impregnated and thermally treated supports were placed in a quartz tube inside a tubular furnace under gas flow of 45 mL/min of H₂S/H₂ mixture (15 % H₂S). Temperature was raised from ambient to 400 °C with a heat rate of 4 °C/min, and kept under these conditions during 4 h. Afterwards, the solid was transferred to a sealed bottle under a nitrogen atmosphere for later characterization and HDS activity study.

2.3. Oxides and sulfided catalysts characterization.

2.3.1. X-ray diffraction (XRD).

X-ray diffractograms were obtained using a Panalytical Xpert’PRO Power Diffractometer (CuK α radiation, 0.154056 nm) operating at 35 mA, 40 kV, step size of 0.05°, and step time of 500 s. Diffraction patterns were analyzed using standard JCPDS files.

2.3.2. Nitrogen physical adsorption characterization

Nitrogen adsorption and desorption measurements were performed using a Quantachrome apparatus (Autosorb-1) at $-196\text{ }^{\circ}\text{C}$ after degasification of at $120\text{ }^{\circ}\text{C}$ for 12 h for oxides, while support and sulfided catalyst were outgassed at 250°C for 8 h. The specific surface area (S_{BET}) was calculated from the BET (Brunauer-Emmett-Teller) method, and the pore-size distribution and pore volume was obtained using the BJH (Barret-Joyner-Halenda) method. The normalized S_{BET} (NS_{BET}) was calculated according to the following equation (Equation 1) [25].

$$NS_{\text{BET}} = \frac{S_{\text{BET of catalyst}}}{[(1-y)*S_{\text{BET of support}}]} \quad \text{Equation 1}$$

Where y , is the content fraction of precursors, metal oxides or metal sulfides, depending on the step during catalyst synthesis.

2.3.3. Transmission electron microscopy (TEM)

The morphology and microstructure of materials were determined by transmission electron microscopy using a Hitachi TM 7700 microscope with a tungsten filament at an accelerating voltage of 100kV. Samples were suspended in 2-propanol and sonicated; then a drop was added on a copper grid coated with lacey carbon. The length and stacking number of the MoS_2 slabs were calculated from at least 500 crystals from each catalyst. All measurements were made with the software Image Pro Plus version 6.0 and the obtained average value was used to calculate the Mo dispersion (f_{Mo}) using equations 2 and 3.

$$f_{\text{Mo}} = \frac{\sum_{i=1}^t (6n - 6)}{\sum_{i=1}^t (3n^2 - 3n + 1)} \quad \text{Equation 2}$$

$$n = \frac{L}{6.4} + 0.5 \quad \text{Equation 3}$$

Where t is the number of layers, n is the number of Mo atoms in one edge, and L is the length of MoS₂ crystals. The molybdenum dispersion (f_{Mo}) was calculated assuming that crystals of MoS₂ are perfect hexagons [27].

2.3.4. X-ray photoelectron spectroscopy (XPS)

X-Ray Photoelectron Spectroscopy (XPS) measurements were performed with a Thermo Scientific Escalab 250Xi spectrometer, samples were analyzed under vacuum ($<10^{-9}$ mbar) with a monochromatic Al K α (1486.6 eV) X-ray source and a spot size of 650 μm , and the binding energies (BE) were recorded taking C1s (284.8 eV) as reference. The Mo3d, Co2p and S2p spectra were analyzed applying a Shirley background subtraction and mixed Gaussian-Lorentzian functions. Surface atomic ratios were calculated from the peak area ratios normalized by their atomic sensitivity factors. For S2s the binding energies and peak areas were constrained by the Equation 4, as previously reported Chen et al. [34].

$$BE(S2s) = BE(S2p_{3/2}) + 64.3, \quad Area(S2s) = Area(S2p) * 0.66$$

Equation 4

The molybdenum, cobalt and sulfur surface atomic concentration [C(Mo), C(Co) and C(S)] for each species was calculated through the Equation 5.

$$C(i)_s = \frac{A_i/SF_i}{\sum_{i=1}^n A_i/SF_i} * 100$$

Equation 5.

Where $C(i)_s$ is the species atomic concentration, A_i is the measured spectra area from the different species, SF_i is the sensitivity factor of each element.

On the other hand, the percentages of Mo species (Mo⁺⁴, ⁺⁵ or ⁺⁶) were calculated using the Equation 6.

$$MoS_2 o Mo^{4+}(\%) = \frac{A_{Mo^{4+}}}{A_{Mo^{4+}} + A_{Mo^{5+}} + A_{Mo^{6+}}} * 100$$

Equation 6.

Similarly, the Co species (CoMoS, Co₉S₈ and Co²⁺) were obtained by Equation 7.

$$\text{CoMoS}(\%) = \frac{A_{\text{CoMoS}}}{A_{\text{CoMoS}} + A_{\text{Co}_9\text{S}_8} + A_{\text{Co}^{2+}}} * 100$$

Equation 7.

2.3.5. Raman spectroscopy

Raman spectra were obtained using a Renishaw inVia Raman Microscope, the single-line laser at 244 nm from an Ar ion laser was used as the Raman excitation source for recording the spectra, the samples were placed in an aluminum capsule to perform the analysis and data acquisition was collected after 30 min of laser exposure time. The spectrum was normalized, and the background was removed for further comparison of intensities.

2.4. Catalytic performance tests

HDS reaction was performed in a high-pressure batch reactor (Parr model 4842). Activity tests were made adding catalyst (0.5 g) into the reactor vessel with a solution of DBT (Sigma Aldrich 98 %, 119.3 mmol/L) in decahydronaphthalene (Sigma-Aldrich, 99%, 4250 ppm of sulfur). The reaction was carried out at 350 °C and under 3.4 MPa of H₂ pressure for 5 h and maintaining constant stirring of 600 rpm. Liquid samples were taken every 30 minutes during the 5 h. Samples were analyzed in a gas chromatograph coupled with mass spectrometer from Shimadzu, GCMS-QP2010 SE equipped with a capillary column RX-1-5Sil MS, length of 30 m and 0.25 mm of diameter. The catalytic performance of the catalysts towards the HDS of DBT was measured by calculating the kinetic rate constants, assuming a pseudo-first order kinetics. The calculations were based on the changes in the concentration of DBT present in the aliquots taken from the reaction system at intervals of 30 min starting when the

temperature of the reactor reached 350 °C. The DBT conversion was calculated as follows [35]:

$$X_{DBT} = \frac{C_{DBT_0} - C_{DBT_i}}{C_{DBT_0}} \quad \text{Equation 8}$$

where C_{DBT_0} is initial molar concentration of DBT (molL^{-1}) and C_{DBT_i} is DBT molar concentration at a determined time i .

Reaction rate constant was calculated using a pseudo-first order kinetic as follows [35]:

$$r_a = kC_{DBT_i} = kC_{DBT_0}(1 - X_{DBT}) \quad \text{Equation 9}$$

The pseudo-first order rate constant is obtained from [35]:

$$kt = -\ln(1 - X_{DBT}) \quad \text{Equation 10}$$

where r_a is the rate constant ($\text{mols}^{-1}\text{g}^{-1}$), k is rate constant (s^{-1}), t is time, and X_{DBT} is DBT conversion.

The HYD/HDS selectivity is calculated using the following equation:

$$S_{HYD/HDS} = \frac{C_{CHB} + C_{DCH} + C_{THDBT}}{C_{BP}} \quad \text{Equation 11}$$

Where C_{CHB} , C_{DCH} , C_{THDBT} and C_{BP} are the CHB, DCH, THDBT and BP concentrations in reaction product, respectively

3. Results and discussion

3.1 Characterization of KIT-6 support and catalysts.

3.1.1. X-ray diffraction analysis.

To confirm the KIT-6 structure, low angle X-ray diffraction was taken from synthesized supports. Figure 1 shows the KIT-6 low angle X-ray diffraction pattern. As can be seen, XRD pattern shows a sharp intense peak at $2\theta = 0.95$ corresponding to (211) plane and $2\theta = 1.1$ a hump attributed to (220) plane. The XRD pattern clearly indicates that material presents an ordered mesoporous structure and belongs to bicontinuous cubic space group Ia3d [4, 33, 36].

The unit cell parameter a_0 of calcined sample was also calculated, getting values of 227.7 Å (211) and 195.7 Å (220), which are in good agreement with the reported in the literature and suggests that mesoporous silica is KIT-6 with body centered cubic symmetry [4].

Powder X-ray diffractograms of the pre-activated catalysts O-135, O-225, O-300, O-450 and O-500 are presented in Figure 1 (b). All samples showed the broad signal between 16° and 30° 2θ typical for amorphous silica [36, 37]. The materials calcined at 450 and 500 °C show major broad diffraction peaks at 2θ values of 23.3, 26.4 and 27.2° . The presence of these peaks could be attributed to the Mo species and the peaks intensity is related to degree of crystallinity in each material, which increases at a higher temperature. The diffraction peaks at 2θ value of 23.4, 25.7 and 27.3° correspond to (110), (040) and (021) planes of the orthorhombic crystalline phase of MoO_3 (ICDD PDF No. 00-076-1003) [38,39]. The additional peaks could be associated to Mo forms like MoO_3 or even MoO_2 . Therefore, the presence of these peaks depicts an additional evidence of the successful impregnation of the KIT-6 with the metal species. There are no evident peaks that indicate the Co presence; this could be explained with the low content of Co with respect to Mo [40]. X-ray diffraction patterns of activated catalysts C-135, C-225, C-300, C-450 and C-500 are showed in Figure 1 (c). In all catalysts, there are four major broad diffraction peaks at 2θ values of 14.5, 33.4, 38.2 and 58.5° which correspond to (002), (100), (103) and (110) plane of the MoS_2 hexagonal-phase (ICDD PDF No. 00-037-1492) [36,41]. As expected, the intensity of the MoS_2 peaks increased with the increase of calcination temperature, indicating the formation of more agglomerated MoS_2 nano-particles at higher calcination temperature [41, 42].

3.1.2. Textural characterization.

A surface area of 647 m^2/g was determined for KIT-6 by nitrogen adsorption, and as expected (Table 2), this support presents type IV adsorption-desorption isotherm corresponding to

mesoporous materials with H1 hysteresis loops for cylindrical pores. KIT-6 has a pore volume of 1.3 cc/g and a pore diameter of 69 Å, which was calculated by the BJH method.

The pre-activated catalysts, i.e., supports impregnated and thermally treated, shown the same kind of adsorption-desorption isotherms and hysteresis, indicating that the mesoporous structure remains unaltered (Figure 2), however, the specific surface area presents a significant reduction of around 200 m²/g (Table 2). Nevertheless, among the pre-activated catalysts an increase in specific surface area was observed as temperature of thermal treatment increases, this could be explained as result of precursor degradation at higher temperatures, thus samples O-450 and O-500 has better textural properties, 430 m²/g and 0.9 cc/g for S_{BET} and pore volume, respectively, due to the release of ammonia and water from cobalt and molybdenum precursors molecules, reducing obstructions into available pores of support.

The average pore diameter from pre-activated and sulfided samples remains close to the pure support value, around 66 Å as shown Table 2, which allows assuming that pores were not internally covered by deposition of multi-layers of precursors, and surface area reduction is mainly due to complete obstruction of some pores. Even more, the same behaviour was detected in specific surface area and pore volume. To determine the specific surface area reduction from the support to pre-activated materials and sulfided catalysts, the NS_{BET} was calculated from Equation 1. For each NS_{BET}, (1-y) value must be calculated considering on whether dispersed cobalt and molybdenum are precursors oxides or sulfided species, the NS_{BET} values are summarized in

Table 2. The obtained values are between 0.77 to 0.82 for pre-activated materials, while after activation NS_{BET} values are from 0.67 to 0.75. Accordingly, to López-Mendoza et al. [32], values near to 0.9 are characteristic of high-dispersed catalysts, while values below 0.6

indicates that a fraction of pores was obstructed by species dispersed on support. The reduction of NS_{BET} values after activation, despite the higher contribution of surface area from higher fraction of support (1-y), indicates that sulfided species obstruct a higher amount of surface originally available on pores of KIT-6.

3.1.3 Raman Spectroscopy.

The collected Raman spectra of pre-activated samples are shown in Figure 3, which were normalized in order to compare the intensity of signals among the studied materials. All samples exhibit a broad peak at 970 cm^{-1} attributed to large polymolybdate clusters such as $Mo_8O_{26}^{4-}$ (Mo=O Raman band of octahedral coordination) [43,44] and also present the signal at 875.7 cm^{-1} associated to Mo-O-Co stretching vibrations in $CoMoO_4$ species (in which cobalt ions are placed in an octahedral environment). These latter species are often related to a decrease in HDS catalytic activity, since is widely known that $CoMoO_4$ cannot be easily transformed into the $CoMoS$ phase [44]. Additionally, the signal located at 690 cm^{-1} related to Co-O stretching vibrations [45] in the oxide state, have been detected in all samples. At $1,065\text{ cm}^{-1}$ a small signal due to nitrate residue from the cobalt precursor has been observed, this signal is not detected at highest temperature treatments, since nitrates decompose around $300\text{ }^\circ\text{C}$.

3.2. Characterization of sulfided catalysts

3.2.1. Active Phase Morphology.

The TEM study is focused on the study of the active phase obtained after activation treatment of catalyst supported on KIT-6. Figure 4 shows TEM micrographs of materials, showing the typical morphology of MoS_2 fringes, the insets present the length distribution of MoS_2 crystals, with Gaussian curve fit. The length and stacking average are summarized in Table 3, both length and stacking tend to increase as the drying temperature increases. For catalyst C-

135 the average stacking degree is the smallest (3.15 layers) of the catalysts series with an average length of 4.23 nm, whereas the longest crystal corresponds to C-500 with 5.19 nm and 3.9 MoS₂ sheets. The average length and stacking are associated to dispersion of Mo atoms available to carry out HDS reaction. The average fraction of Mo atoms on the edge surface (f_{Mo}) is a Mo dispersion indicator, which is calculated from Equation 2 and Equation 3. The Table 3 shows the obtained f_{Mo} values, and as can be seen, higher dispersion is obtained at lower temperature of thermal treatment, except for C-450.

3.2.2. XPS analysis of activated catalysts.

The surface chemical states of metal species on the sulfided catalysts were investigated by XPS spectroscopy. The Mo3d spectra of catalysts are presented in Figure 5, showing the doublets corresponding to the contributions of Mo 3d_{5/2} and Mo 3d_{3/2} of different Mo species such as sulfided (Mo⁺⁴), partially sulfided (Mo⁺⁵) and oxidized (Mo⁺⁶) [43,46,47], additionally, a single signal is also presented from S2s at 226.0 eV. The spectra deconvolution shows the presence of Mo species at 228.4 and 232.2 eV, which correspond to Mo⁴⁺3d_{5/2} and Mo⁴⁺3d_{3/2}, respectively. Doublets at 230.9 and 234.1 eV correspond to MoS_xO_y species; while at 234.3 and 237.2 eV the signals are associated with MoO_x polymorphs. The Co2p spectra were also collected, and the corresponding deconvolution are presented in Figure 6. The contribution from different Co species was observed, Co₉S₈ at 777.8 eV, CoMoS at 780.2 eV, being the latter commonly considered responsible of most of HDS activity, therefore it is the most expected species, and finally, Co⁺² from CoO_x at 782.9 eV and the satellite of Co⁺². From XPS spectra, differences on signals intensity were observed. Table 4 shows molybdenum and cobalt percentage present in the catalysts. The main difference is related whit molybdenum composition (specifically Mo⁺⁴), obtaining 36 y 25 % for C-500 and C-135, respectively. Similar behaviour is observed from CoMoS content,

reaching 41 % for C-500, and 33 % for C-135 catalyst. The catalyst with highest sulfidation degree is the calcined at 500 °C, this temperature could improve the formation of MoS₂ and hence the mayor formation of CoMoS phase.

3.2.3. Hydrodesulfuration of Dibenzothiophene.

The effect of calcination temperature over the hydrodesulfurization activity of the catalysts C-135, C-225, C-300, C-450 and, C-500 was studied through the HDS reaction, using DBT as a model molecule. DBT conversion, reaction rate constant and selectivity were calculated using equations 8, 10 and 11, respectively; the results are presented in Table 5. A reduction in the DBT conversion was observed as follows 71% (C-135) > 65% (C-225) > 62% (C-300) > 61% (C-450) > 58% (C-500). According to the literature [1–4], the HDS of DBT occurs through two desulfurization parallel routes: direct desulfurization (DDS) and hydrogenation (HYD). On DDS path, sulfur is removed by hydrogenolysis of C-S bond without aromatic ring hydrogenation producing biphenyl (BP). On the other hand in the hydrogenation route (HYD), aromatic ring saturation is required before the desulfuration step, producing intermediate compounds such as tetra hydrodibenzothiophene (THDBT). Once sulfur is removed, then cyclohexylbenzene (CHB) and dicyclohexyl (DCH) are generated. The DDS was the main route observed for studied catalysts, since the principal product detected was biphenyl (BP). In Table 5 the correlation between the drying temperature and selectivity is summarized, no significant effect was detected over selectivity on the catalyst HDS, since the selectivity values were comparable (0.35-0.36). According to the HDS catalytic results, C-135 has the highest reaction rate constant 21×10^{-7} mol/s•g, and the lowest is 15×10^{-7} mol/s•g for C-500 catalyst. Considering these results, the increment in the temperature of pre-activation thermal treatment leads to a reduction of the catalytic activity of the catalyst.

3.3. Discussion

According to catalytic activity results, the best HDS performance was obtained for the catalyst that was thermally treated at 135 °C, this enhanced performance was due to the combination of several factors such as a good Mo dispersion ($f_{\text{Mo}}=0.28$), smaller MoS₂ crystals (4 nm) and low stacking degree (3 slabs), as well as to have 95 % of MoS₂ promoted with cobalt, and those characteristics allowed to obtain a rate constant of 21×10^{-7} mol/g·s. On the other hand, the catalyst C-500 showed the lowest HDS activity, the poor performance could be attributed to a poor Mo dispersion ($f_{\text{Mo}}=0.23$) derived from the average length of crystals (5 nm), despite all the other characteristics are very close to the values of C-135.

Raman spectra for all catalyst presented a small signal of CoMoO₄, which is not desirable in HDS catalyst synthesis; the strongest signal shown in the spectra was Mo₈O₂₆⁴⁺. These results along with Mo dispersion and the ratios of CoMoS/MoS₂ are the best prediction to a highly active catalyst.

In order to explain more profoundly the differences observed in the obtained materials, a thermogravimetric analysis of the Mo precursor (HMA) used for the impregnation of the catalysts was carried out. The thermogram obtained is shown in Figure 7. Total weight loss of 18.6% can be observed as a result of calcination until 500 °C. The HMA precursor degradation is carried out in three steps, the first step occurs with a 7% weight loss in which ammonia is released; according to the work of Said et al. [47,48], second and third steps consist on the elimination of chemically bound water, with weight losses of 4 and 7.6% for each case. The degradation reactions are carried out at 110, 210 and 290 °C. This allows considering that the present species in materials treated at low temperatures are related to high coordination molybdenum-hydrated molecules, while the MoO₃ species start to appear after 210 °C until becoming the only phase at 500 °C. The decrease in the magnitude of the rate constant as the calcination temperature increases is a clear indication that calcination at higher temperatures reduces the activity of the catalysts. The observed phenomenon could be

attributed to the higher crystallinity degree of MoO₃ species at higher temperatures, which is evident in the XRD patterns (Figure 1) and therefore, sulfidation becomes more difficult.

4. Conclusion.

In this work, CoMo catalysts, supported over mesoporous silica (KIT-6) were prepared through a thermal treatment before activation of impregnated cobalt and molybdenum precursors on KIT-6 support, and the resulting efficiency was measured in DBT desulfurization. According to HDS catalytic results, the best catalyst was obtained at the lower temperature used for the thermal treatment, before activation (135 °C); higher temperatures used for other catalysts do not improve the activity results. Thus, thermal treatment after drying step and before activation become an easy way to improve HDS activity of a catalyst. Raman study of species formed during pre-activation thermal treatment and XPS and TEM analyses of active phases formed after activation treatment allows understanding catalytic properties of studied materials from the information of species formed in each step and the dispersion and structures of CoMoS active phase dispersed on KIT-6 support.

Declaration of interests

- The authors declare that they have no known competing financial interests or personal relationships that could have appeared to influence the work reported in this paper.
- The authors declare the following financial interests/personal relationships which may be considered as potential competing interests:

Acknowledgement.

The authors gratefully acknowledge the technical support of Raúl Ochoa, Luis Silva, Luis de la Torre and Dr. Victor Ramos. The authors appreciatively acknowledge the Mexican Council of Science and Technology (CONACYT) for support through the projects “Laboratorio Nacional de Micro y Nanofluídica“ no. 293442 and CONACYT-SENER-Hidrocarburos No. 120135.

References

- [1] I. Babich, Science and technology of novel processes for deep desulfurization of oil refinery streams: a review*, *Fuel*. 82 (2003) 607–631. doi:10.1016/S0016-2361(02)00324-1.
- [2] H. Wu, A. Duan, Z. Zhao, D. Qi, J. Li, B. Liu, et al., Preparation of NiMo/KIT-6 hydrodesulfurization catalysts with tunable sulfidation and dispersion degrees of active phase by addition of citric acid as chelating agent, *Fuel*. 130 (2014) 203–210. doi:10.1016/j.fuel.2014.04.038.
- [3] T. Fujikawa, H. Kimura, K. Kiriya, K. Hagiwara, Development of ultra-deep HDS catalyst for production of clean diesel fuels, *Catal. Today*. 111 (2006) 188–193. doi:10.1016/j.cattod.2005.10.024.
- [4] K. Soni, B.S. Rana, A.K. Sinha, A. Bhaumik, M. Nandi, M. Kumar, et al., 3-D ordered mesoporous KIT-6 support for effective hydrodesulfurization catalysts, *Appl. Catal. B Environ*. 90 (2009) 55–63. doi:10.1016/j.apcatb.2009.02.010.
- [5] C. Song, An overview of new approaches to deep desulfurization for ultra-clean gasoline, diesel fuel and jet fuel, *Catal. Today*. 86 (2003) 211–263. doi:10.1016/S0920-5861(03)00412-7.
- [6] J. Ramirez, F. Sanchez-Minero, Support effects in the hydrotreatment of model molecules, *Catal. Today*. 130 (2008) 267–271. doi:10.1016/j.cattod.2007.10.103.
- [7] A. Rochet, B. Baubet, V. Moizan, E. Devers, A. Hugon, C. Pichon, et al., Influence of the Preparation Conditions of Oxidic NiMo/Al₂O₃ Catalysts on the Sulfidation Ability: A Quick-XAS and Raman Spectroscopic Study, *J. Phys. Chem. C*. 119 (2015) 23928–23942. doi:10.1021/acs.jpcc.5b06219.
- [8] M. Breyse, P. Afanasiev, C. Geantet, M. Vrinat, Overview of support effects in hydrotreating catalysts, *Catal. Today*. 86 (2003) 5–16. doi:10.1016/S0920-

- 5861(03)00400-0.
- [9] H. YIN, T. ZHOU, Y. LIU, Y. CHAI, C. LIU, Study on the structure of active phase in NiMoP impregnation solution using Laser Raman spectroscopy II. Effect of organic additives, *J. Fuel Chem. Technol.* 39 (2011) 109–114. doi:10.1016/S1872-5813(11)60012-1.
- [10] Y. Espinoza-Armenta, J. Cruz-Reyes, F. Paraguay-Delgado, M. Del Valle, G. Alonso, S. Fuentes, et al., CoMoW sulfide nanocatalysts for the HDS of DBT from novel ammonium and alkyltrimethylammonium-thiomolybdate-thiotungstate-cobaltate (II) precursors, *Appl. Catal. A Gen.* 486 (2014) 62–68. doi:10.1016/j.apcata.2014.08.017.
- [11] F. Trejo, M. Rana, J. Ancheyta, CoMo/MgO–Al₂O₃ supported catalysts: An alternative approach to prepare HDS catalysts, *Catal. Today.* 130 (2008) 327–336. doi:10.1016/j.cattod.2007.10.105.
- [12] S. a. Hanafi, M.S. Mohamed, Recent Trends in the Cleaning of Diesel Fuels via Desulfurization Processes, *Energy Sources, Part A Recover. Util. Environ. Eff.* 33 (2011) 495–511. doi:10.1080/15567030903058360.
- [13] R.R. Chianelli, A.F. Ruppert, S.K. Behal, B.H. Kear, A. Wold, R. Kershaw, The reactivity of MoS₂ single crystal edge planes, *J. Catal.* 92 (1985) 56–63. doi:10.1016/0021-9517(85)90236-2.
- [14] R.R. Chianelli, G. Berhault, B. Torres, Unsupported transition metal sulfide catalysts: 100 years of science and application, *Catal. Today.* 147 (2009) 275–286. doi:10.1016/j.cattod.2008.09.041.
- [15] M. Ramos, F. Galindo-Hernández, I. Arslan, T. Sanders, J.M. Domínguez, Electron tomography and fractal aspects of MoS₂ and MoS₂/Co spheres, *Sci. Rep.* 7 (2017) 12322. doi:10.1038/s41598-017-12029-8.
- [16] C. Kwak, J.J. Lee, J.S. Bae, K. Choi, S.H. Moon, Hydrodesulfurization of DBT, 4-

- MDBT, and 4,6-DMDBT on fluorinated CoMoS/Al₂O₃ catalysts, *Appl. Catal. A Gen.* 200 (2000) 233–242. doi:10.1016/S0926-860X(00)00635-9.
- [17] M. EGOROVA, R. PRINS, The role of Ni and Co promoters in the simultaneous HDS of dibenzothiophene and HDN of amines over Mo/ γ -Al₂O₃ catalysts, *J. Catal.* 241 (2006) 162–172. doi:10.1016/j.jcat.2006.04.011.
- [18] T.C. Ho, Deep HDS of diesel fuel: chemistry and catalysis, *Catal. Today.* 98 (2004) 3–18. doi:10.1016/j.cattod.2004.07.048.
- [19] R. Shafi, G.J. Hutchings, Hydrodesulfurization of hindered dibenzothiophenes: an overview, *Catal. Today.* 59 (2000) 423–442. doi:10.1016/S0920-5861(00)00308-4.
- [20] A. Stanislaus, A. Marafi, M.S. Rana, Recent advances in the science and technology of ultra low sulfur diesel (ULSD) production, *Catal. Today.* 153 (2010) 1–68. doi:10.1016/j.cattod.2010.05.011.
- [21] J.A. Mendoza-Nieto, F. Robles-Méndez, T.E. Klimova, Support effect on the catalytic performance of trimetallic NiMoW catalysts prepared with citric acid in HDS of dibenzothiophenes, *Catal. Today.* 250 (2015) 47–59. doi:10.1016/j.cattod.2014.05.002.
- [22] M.J. Girgis, B.C. Gates, Reactivities, reaction networks, and kinetics in high-pressure catalytic hydroprocessing, *Ind. Eng. Chem. Res.* 30 (1991) 2021–2058. doi:10.1021/ie00057a001.
- [23] P. a. Nikulshin, V. a. Salnikov, A.V. Mozhaev, P.P. Minaev, V.M. Kogan, A. a. Pimerzin, Relationship between active phase morphology and catalytic properties of the carbon–alumina-supported Co(Ni)Mo catalysts in HDS and HYD reactions, *J. Catal.* 309 (2014) 386–396. doi:10.1016/j.jcat.2013.10.020.
- [24] D. Laurenti, B. Phung-Ngoc, C. Roukoss, E. Devers, K. Marchand, L. Massin, et al., Intrinsic potential of alumina-supported CoMo catalysts in HDS: Comparison between γ c, γ T, and δ -alumina, *J. Catal.* 297 (2013) 165–175. doi:10.1016/j.jcat.2012.10.006.

- [25] R. Huirache-Acuña, B. Pawelec, C.V. Loricera, E.M. Rivera-Muñoz, R. Nava, B. Torres, et al., Comparison of the morphology and HDS activity of ternary Ni(Co)-Mo-W catalysts supported on Al-HMS and Al-SBA-16 substrates, *Appl. Catal. B Environ.* 125 (2012) 473–485. doi:10.1016/j.apcatb.2012.05.034.
- [26] M. a. Guzmán, R. Huirache-Acuña, C.V. Loricera, J.R. Hernández, J.N. Díaz de León, J. a. de los Reyes, et al., Removal of refractory S-containing compounds from liquid fuels over P-loaded NiMoW/SBA-16 sulfide catalysts, *Fuel.* 103 (2013) 321–333. doi:10.1016/j.fuel.2012.07.005.
- [27] O.Y. Gutiérrez, T. Klimova, Effect of the support on the high activity of the (Ni)Mo/ZrO₂-SBA-15 catalyst in the simultaneous hydrodesulfurization of DBT and 4,6-DMDBT, *J. Catal.* 281 (2011) 50–62. doi:10.1016/j.jcat.2011.04.001.
- [28] D. Valencia, T. Klimova, Citric acid loading for MoS₂-based catalysts supported on SBA-15. New catalytic materials with high hydrogenolysis ability in hydrodesulfurization, *Appl. Catal. B Environ.* 129 (2013) 137–145. doi:10.1016/j.apcatb.2012.09.006.
- [29] T.E. Klimova, D. Valencia, J.A. Mendoza-Nieto, P. Hernández-Hipólito, Behavior of NiMo/SBA-15 catalysts prepared with citric acid in simultaneous hydrodesulfurization of dibenzothiophene and 4,6-dimethyldibenzothiophene, *J. Catal.* 304 (2013) 29–46. doi:10.1016/j.jcat.2013.03.027.
- [30] S. Badoga, K.C. Mouli, K.K. Soni, A.K. Dalai, J. Adjaye, Beneficial influence of EDTA on the structure and catalytic properties of sulfided NiMo/SBA-15 catalysts for hydrotreating of light gas oil, *Appl. Catal. B Environ.* 125 (2012) 67–84. doi:10.1016/j.apcatb.2012.05.015.
- [31] M.Á. Calderón-Magdaleno, J.A. Mendoza-Nieto, T.E. Klimova, Effect of the amount of citric acid used in the preparation of NiMo/SBA-15 catalysts on their performance

- in HDS of dibenzothiophene-type compounds, *Catal. Today*. 220–222 (2014) 78–88. doi:10.1016/j.cattod.2013.06.002.
- [32] M.A. López-Mendoza, R. Nava, C. Peza-Ledesma, B. Millán-Malo, R. Huirache-Acuña, P. Skewes, et al., Characterization and catalytic performance of Co-Mo-W sulfide catalysts supported on SBA-15 and SBA-16 mechanically mixed, *Catal. Today*. 271 (2016) 114–126. doi:10.1016/j.cattod.2015.07.049.
- [33] F. Kleitz, S. Hei Choi, R. Ryoo, Cubic Ia3d large mesoporous silica: synthesis and replication to platinum nanowires, carbon nanorods and carbon nanotubes Electronic supplementary information (ESI) available: TEM images of mesoporous cubic silica and Pt networks, XRD patterns during forma, *Chem. Commun.* (2003) 2136. doi:10.1039/b306504a.
- [34] W. Chen, X. Long, M. Li, H. Nie, D. Li, Influence of active phase structure of CoMo/Al₂O₃ catalyst on the selectivity of hydrodesulfurization and hydrodearomatization, *Catal. Today*. 292 (2017) 97–109. doi:10.1016/j.cattod.2016.09.029.
- [35] I. Vázquez, A. López, G. Berhault and A. Guevara, Effect of support on the acidity of NiMo/Al₂O₃-MgO and NiMo/TiO₂-Al₂O₃ catalysts and on the resulting competitive hydrodesulfurization/hydrodenitrogenation reactions, *Fuel*. 236 (2019) 55-64. doi:10.1016/j.fuel.2018.08.053.
- [36] A.D. Delgado, L. Alvarez Contreras, K.A. Beltrán, A. Aguilar Elguezabal, Effect of the SiO₂ support morphology on the hydrodesulfurization performance of NiMo catalysts, *J. Mater. Res.* 33 (2018) 3646–3655. doi:10.1557/jmr.2018.382
- [37] F. Kleitz, S. H. Choi and R. Ryoo, “Cubic Ia3d large mesoporous silica: synthesis and replication to platinum nanowires, carbon nanorods and carbon nanotubes,” *Chemical communications* (Cambridge, England), (2003) 2136–2137. doi:10.1039/b306504a

- [38] F. Méndez, G. Ascención, M. Mota, I. Lee, X. Bokhimi and T.E. Klimova, “NiMo catalysts supported on Al, Nb, Ti or Zr-containing MCM-41 for dibenzothiophene hydrodesulfurization” *Catal. Today*, 2010 (2018). doi:10.1016/j.cattod.2018.03.039
- [39] International Center for Diffraction Data, PCPDFWIN v.2.02. PDF-2 Data Base, Newtown Philadelphia, (1995).
- [40] T. C. Ho, “Deep HDS of diesel fuel: chemistry and catalysis”, *Catal. Today*, 98 (2008) 3-18. doi:10.1016/j.cattod.2004.07.048
- [41] C. Yin, L Zhao, Z. Bai, H. Liu, Y Liu and C. Liu, " A novel porous ammonium nickel molybdate as the catalyst precursor towards deep hydrodesulfurization of gas oil. " *Fuel*, 107 (2013) 873–878. doi:10.1016/j.fuel.2013.02.001
- [42] H. Liu, C. Yin, B. Liu, X. Li, Y. Li, Y. Chai and C. Liu, “Effect of Calcination Temperature of Unsupported NiMo Catalysts on the Hydrodesulfurization of Dibenzothiophene”, *Energy and Fuels*, 28 (2014) 2429-2436. doi:10.1021/ef500097u
- [43] L. Peña, D. Valencia, T. Klimova, CoMo/SBA-15 catalysts prepared with EDTA and citric acid and their performance in hydrodesulfurization of dibenzothiophene, *Appl. Catal. B Environ.* 147 (2014) 879–887. doi:10.1016/j.apcatb.2013.10.019.
- [44] R. Nava, R.A. Ortega, G. Alonso, C. Ornelas, B. Pawelec, J.L.G. Fierro, CoMo/Ti-SBA-15 catalysts for dibenzothiophene desulfurization, *Catal. Today*. 127 (2007) 70–84. doi:10.1016/j.cattod.2007.02.034.
- [45] P. Mazoyer, C. Geantet, F. Diehl, S. Lorient, M. Lacroix, Role of chelating agent on the oxidic state of hydrotreating catalysts, *Catal. Today*. 130 (2008) 75–79. doi:10.1016/j.cattod.2007.07.013.
- [46] H. Yuan, Q. Herima, G.-T. Xu, H.-F. Li, L.-J. Lu, Study of oxidic and sulfided selective hydrodesulfurization catalysts for gasoline using Raman spectroscopy, *Chinese Chem. Lett.* 24 (2013) 1041–1044. doi:10.1016/j.ccllet.2013.07.009.

- [47] E. Rodríguez-Castellón, A. Jiménez-López, D. Eliche-Quesada, Nickel and cobalt promoted tungsten and molybdenum sulfide mesoporous catalysts for hydrodesulfurization, *Fuel*. 87 (2008) 1195–1206. doi:10.1016/j.fuel.2007.07.020.
- [48] a. F.. Sanders, A.. de Jong, V.H.. de Beer, J. a. . van Veen, J.. Niemantsverdriet, Formation of cobalt–molybdenum sulfides in hydrotreating catalysts: a surface science approach, *Appl. Surf. Sci.* 144–145 (1999) 380–384. doi:10.1016/S0169-4332(98)00831-9.

Journal Pre-proof

Figure Captions

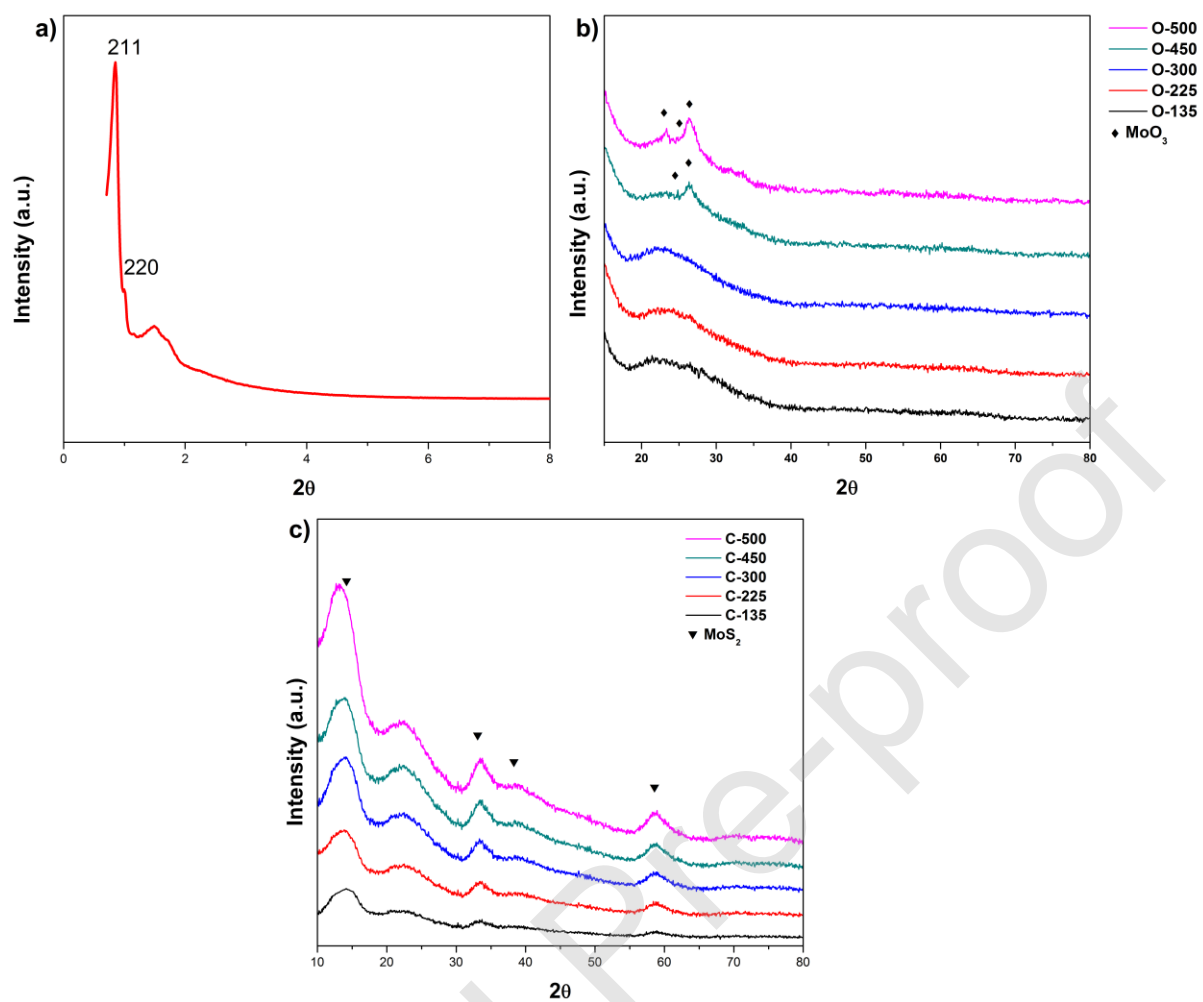


Figure 1. X-Ray diffraction spectra of low angle support (a), pre-activated catalysts (b) and sulfided catalysts (c).

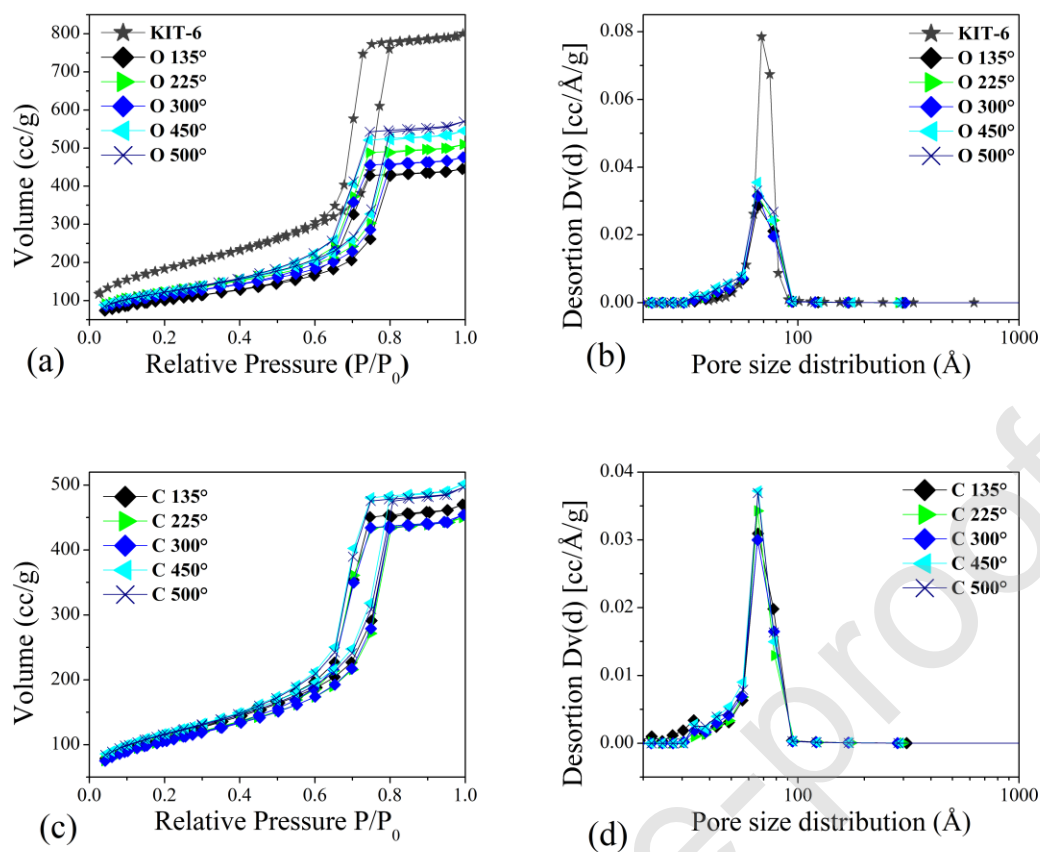


Figure 2. Adsorption-desorption isotherms of support and catalysts in the pre-activated (a) and sulfided state (c), pore size distribution of support and pre-activated catalysts (b) and sulfided catalysts (d).

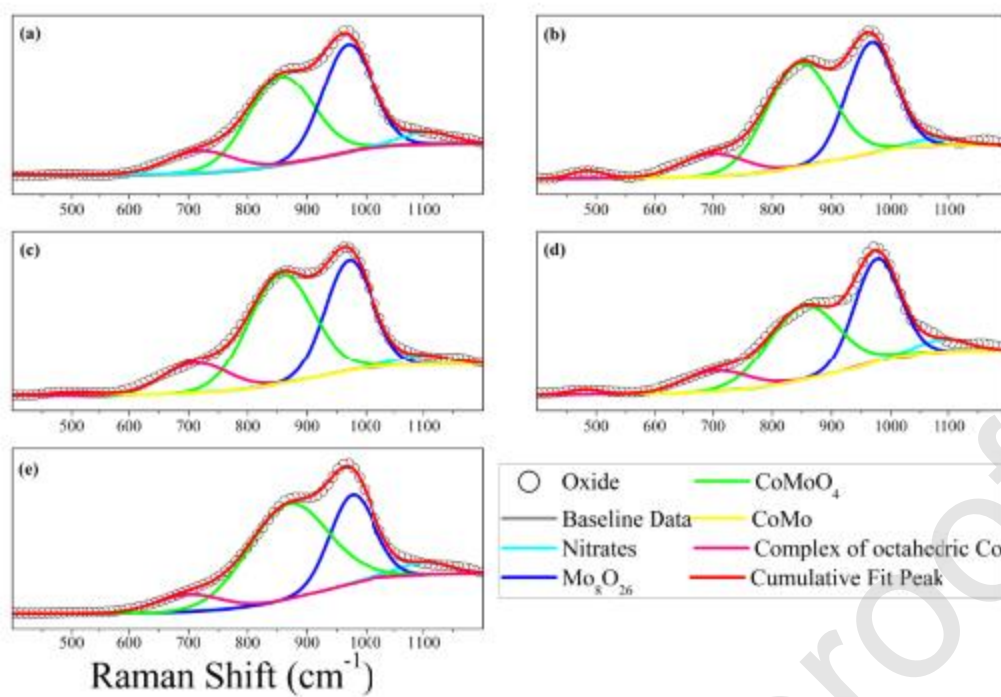


Figure 3. Deconvoluted Raman spectra of pre-activated samples, a) O-135, b) O-235, c) O-300, d) O-450 and e) O-500.

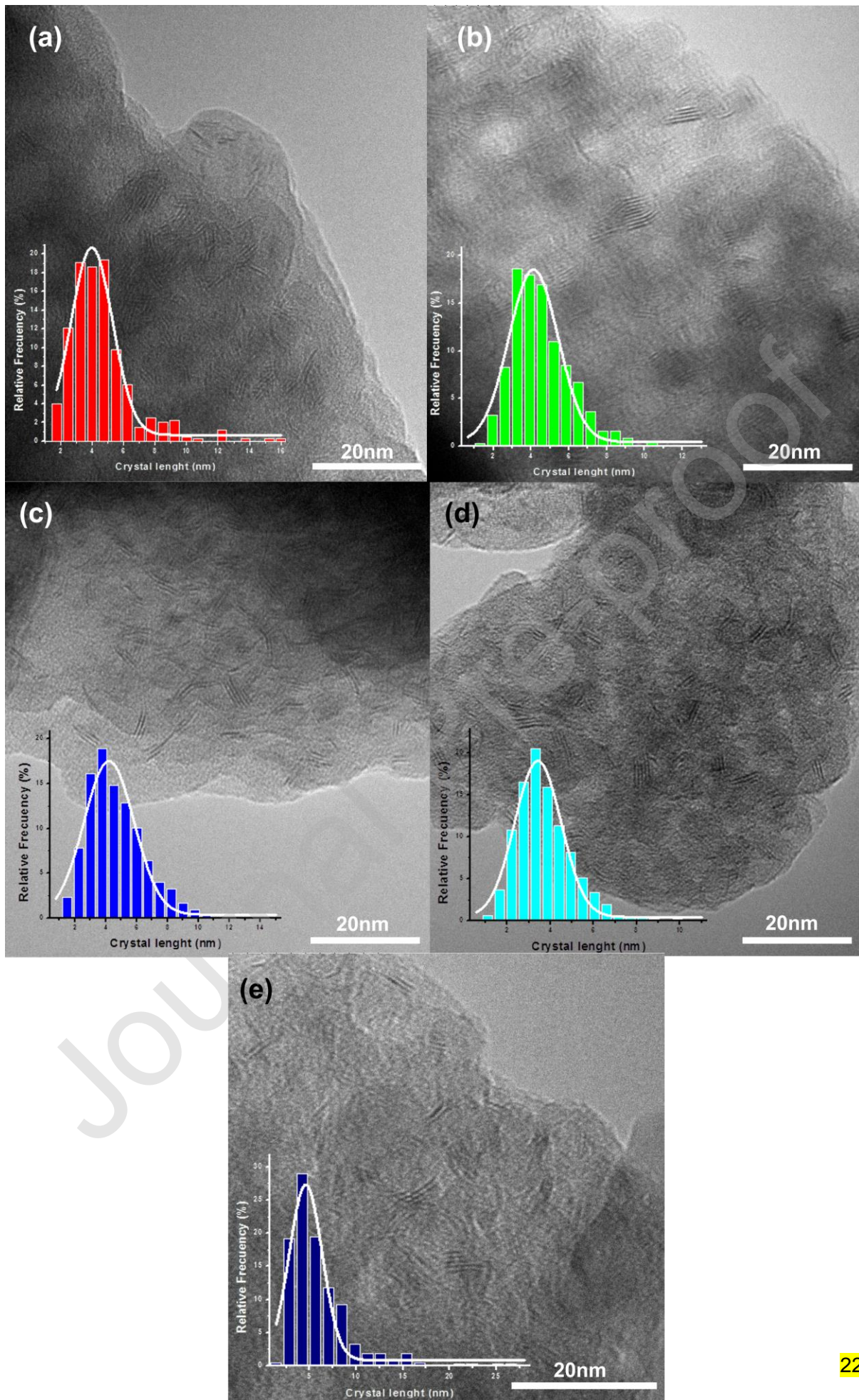


Figure 4. TEM micrographics of sulfided catalysts, a) C-135, b) C-225, c) C-300, d) C-450 and e) C-500. Crystal length distribution (inset)

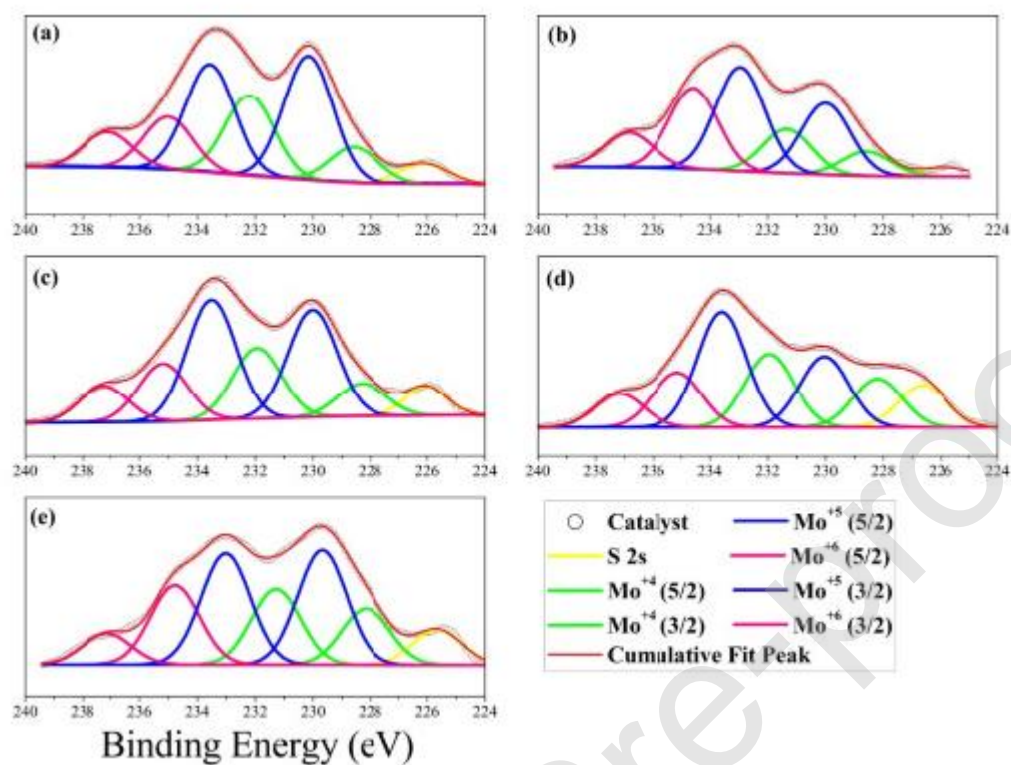


Figure 5. XPS spectra of Mo3d of sulfides catalysts, a) C-135, b) C-225, c) C-300, d) C-450, e) C-500.

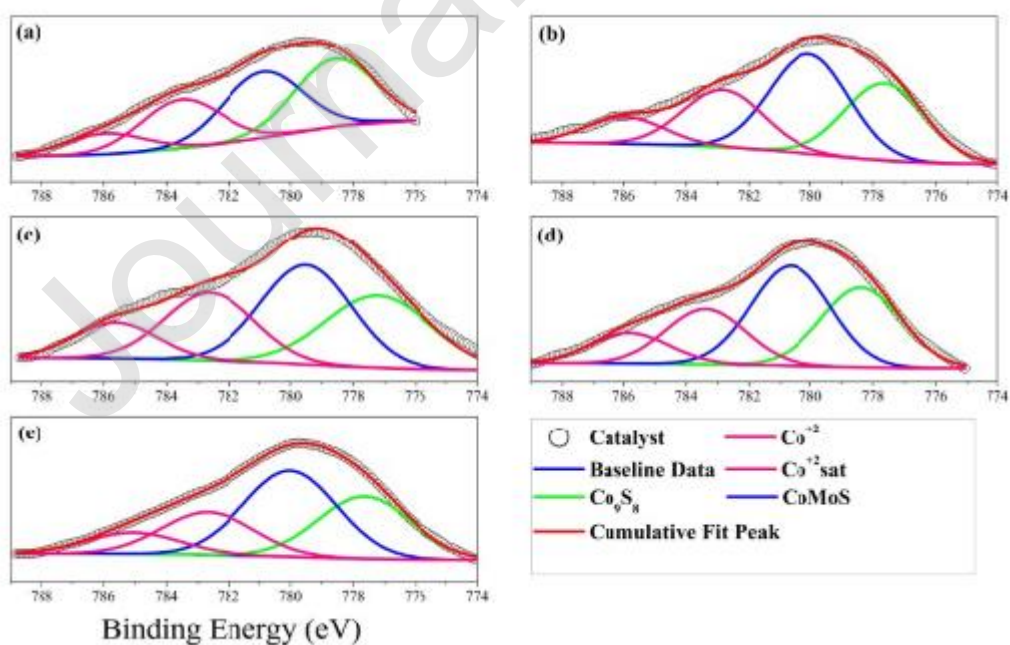


Figure 6. XPS of Co2p of sulfided catalysts a) C-135, b) C-225, c) C-300, d) C-450, e) C-500.

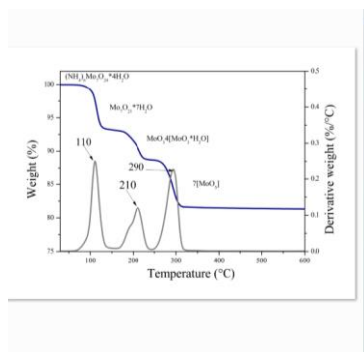


Figure 7. Thermogravimetric analysis from HMA precursor.

Journal Pre-proof

Table 1. Temperature of thermal treatment of impregnated supports to obtain pre-activated materials and their nomenclature.

Sample	Temperature of treatment (°C)
O-135	135
O-225	225
O-300	300
O-450	450
O-500	500

Table 2. Textural properties of support, pre-activated and sulfided catalysts. (1-y) value indicates the fraction of support for each material.

Sample	Surface area m ² /g	Pore volume cc/g	Pore diameter Å	(1-y)	NS _{BET}
KIT-6	647	1.3	69		
O-135	360	0.7	66	0.72	0.77
O-225	424	0.8	66	0.75	0.87
O-300	400	0.7	66	0.80	0.77
O-450	430	0.9	66	0.81	0.82
O-500	430	0.9	65	0.81	0.82
C-135	400	0.8	66	0.85	0.73
C-225	370	0.7	66	0.85	0.67
C-300	370	0.7	66	0.85	0.67
C-450	410	0.8	66	0.85	0.75
C-500	410	0.8	66	0.85	0.75

Table 3. Average length (L), number of layers (N) from MoS₂ phase in CoMo catalysts and average fraction of Mo atoms in the edge surface of the MoS₂ crystals (f_{Mo}).

Catalyst	L	N	Mo _{edge}	Mo _{total}	n	f_{Mo}
	Average length (nm)	Average stacking			Mo-Mo bonds at the edge	
C-135	4.23	3.15	36.7	131.3	7.1	0.28
C-225	4.20	4.65	36.4	129.6	7.1	0.28
C-300	4.31	4.15	37.4	136.1	7.2	0.27
C-450	3.50	3.80	29.4	87.9	5.9	0.33
C-500	5.19	3.90	45.6	197.2	8.6	0.23

Table 4. Binding energies, FWHM in parenthesis and fractions of Co-Mo species in sulfide catalysts.

Catalyst	Mo 3d fractions (%)			Co 2p fractions (%)		
	Mo ⁺⁴	Mo ⁺⁵	Mo ⁺⁶	Co ₉ S ₈	CoMoS	CoO
	228.4±0.24	230.9±0.9	234±0.8	777.8±0.06	780.15±0.06	782.9±0.06
C-135	25 (1.5±0.2)	39 (1.5±0.2)	36 (1.5±0.2)	33 (3)	33 (3)	34 (3)
C-225	26 (2±0.2)	40 (2±0.2)	34 (2±0.2)	30 (3)	38 (3)	32 (3)
C-300	33 (1.7)	45 (1.7)	22 (1.7)	30 (3±1)	35 (3±1)	35 (3±1)
C-450	30 (2±0.3)	47 (2±0.3)	22 (2±0.3)	30 (3)	38 (3)	32 (3)
C-500	36 (2)	40 (2)	24 (2)	29 (3.5)	41 (3.5)	30 (3.5)

Table 5. DBT conversions and products distribution for the HDS reaction of DBT

Catalyst	$k \times 10^{-7}$	DBT ^b conversion	Products distribution ^a				
			THDBT	BP	CHB	DCH	HYD/HDS
	(mol/s·g)	(%)	%			Dimensionless	
C-135	21	71	1.9	42.5	11.4	2.2	0.36
C-225	18	65	1.9	43	10.7	2.4	0.35
C-300	18	62	1.8	42.6	10.2	3.3	0.36
C-450	19	62	1.9	42.6	12.4	1.2	0.36
C-500	15	58	2	43.1	12.4	0.5	0.35

^aProducts distribution and selectivity were calculated at 58% DBT conversion.

^bReaction conditions were: T=350 °C, P_{H₂}=3.4 MPa, t=5 h.